PHYSICAL REVIEW B VOLUME 24, NUMBER 12 15 DECEMBER 1981

Raman scattering by coupled LO-phonon—plasmon modes and forbidden TO-phonon Raman scattering in heavily doped *p*-type GaAs

D. Olego and M. Cardona
Max-Planck-Institut für Festkörperforschung, Heisenbergstrasse 1, 7000 Stuttgart 80, Federal Republic of Germany
(Received 28 July 1981)

Raman scattering by coupled LO-phonon—plasmon modes of *large* wave vectors and *forbidden* TO-phonon Raman scattering have been measured in the first-order Stokes-Raman spectra of (100) surfaces of heavily doped *p*-type GaAs with concentrations ranging from 10^{17} to 10^{20} holes cm^{-3}. The wave-vector nonconservation and the breakdown of the selection rules are due to scattering by the ionized impurities. The measured peak positions, linewidth, and intensities of the LO-like and TO-like Raman lines are explained by postulating a wave-vector distribution of the modes created in the Raman process. Expressions for this wave-vector distribution which depend on the scattering mechanism involved are discussed.

I. INTRODUCTION

Owing to the presence of free carriers in heavily doped semiconductors a strong interaction can take place between the electrons (holes) and the optical phonons. Two forms of interactions can be distinguished: (i) the coupling between single-particle electronic (hole) excitations and transverse-optical phonons and (ii) the coupling between plasmons and longitudinal-optical phonons. Both types of couplings have been extensively studied in the last years using Raman spectroscopy.[1]

The transverse-optical phonons (TO phonons) couple with single-particle electronic excitations through the so-called deformation-potential mechanism. This interaction changes the self-energy of the TO phonons in heavily doped semiconductors and consequently produces a renormalization of their frequencies and lifetimes. These self-energy effects, which are rather small, have been investigated with first-order Raman scattering by measuring shifts and broadenings of the TO Raman lines in the heavily doped material as compared with those lines in a pure sample.[2] Together with the mentioned self-energy effects an asymmetrical broadening of the TO Raman lines was measured in *p*- and *n*-type Si,[3,4] *p*-type Ge,[5,6] and *p*-type GaAs.[5,6] The asymmetrical line shape arises from a coherent discrete-continuum interaction between the one-phonon scattering and a Raman-active continuum of electronic excitations. The electronic continuum interacting with the TO phonons is provided by *direct* inter-valence-band transitions in *p*-type Si (Ref. 3) and *direct* inter-conduction-band transitions in *n*-type Si,[4] while it arises in part from *indirect* transitions between the valence bands in *p*-type Ge and *p*-type GaAs.[5,6] A direct observation of the electronic continuum in the Raman spectra has been reported in the case of *p*-type GaAs.[7]

The longitudinal-optical phonons (LO phonons) couple strongly with collective oscillations of the free-carrier system (plasmons) because of the macroscopic electric fields associated with both kinds of elementary excitations. The dispersion relations of the coupled modes, denoted by $L^{\pm}(\vec{q})$, are well understood by now.[8–10] For vanishing wave vectors $\vec{q}$ the frequency of the L^- modes is less than or equal to the TO phonon frequency, while the frequency of the L^+ modes is greater than or equal to the LO phonon frequency. When the plasma frequency is very small compared with the LO frequency, the L^- modes show a plasmonlike character and the L^+ modes a phononlike one. In the opposite limit (very large free-carrier concentration), L^+ is plasmonlike while L^- has a phononlike behavior. In the latter case the frequency of the L^- modes approaches the TO phonon frequency, which means a nearly complete screening of the electric field of the LO phonon by the free carriers. When the plasmon and LO phonon frequencies become comparable a strong repulsion of the two

modes takes place.

For a given free-carrier concentration the L^+ mode shifts to higher frequencies with increasing wave vector $\vec{q}$ and ceases to exist (it becomes overdamped) soon after penetrating the free-particle excitation region. The L^+ mode becomes Landau damped. The L^- mode shifts also to higher frequencies and approaches the LO phonon frequency within the free-particle excitation spectrum. L^- emerges out of the free-particle excitation spectrum with the LO frequency for wave vectors larger than twice the Fermi wave vector. For these relatively large wave vectors the free carriers are not able to screen the electric field associated with the LO phonons. The dependence of the $L^\pm$ frequencies on free-carrier concentration and their dispersion relations are summarized, respectively, in Fig. 4.3 of Ref. 8 and Figs. 2 and 7 of Refs. 9 and 10.

The coupled plasmon-LO-phonon modes have been investigated mostly in *n*-type semiconductors and particularly in *n*-type GaAs. The resonant behavior of the different scattering mechanisms contributing to the total Raman cross section of the coupled modes has been reported for this material,[11] as well as a detailed study of the corresponding dispersion relations using Raman backscattering techniques.[9] In the latter investigations coupled modes were created in the Raman process with wave vectors given by the $\vec{q}$ transfer of the incident and scattered photons. By changing the energy of the incident photons it is possible to change the wave vector of the elementary excitations created through the relationship between the photon frequency, the frequency-dependent refractive index, and $\vec{q}$.

There have been only very few investigations of the interactions between LO phonons and free holes or their excitations in *p*-type semiconductors as compared with the amount of work on electron-LO-phonon interaction in *n*-type materials and the TO continuum coupling in the *p*-type ones. Fano-type line shapes have been reported recently for the LO phonons of *p*-type GaSb and *p*-type InSb.[12] Coupled LO-phonon–plasmon modes of large wave vector were observed for forbidden configurations in the Stokes-Raman spectra of heavily doped *p*-type GaAs.[13] The large wave vectors were attributed to wave-vector nonconservation due to scattering by the ionized impurities.

The motivation of the present work was to perform a detailed study of the LO-phonon–plasmon coupling in *p*-type GaAs for a wide range of free-hole concentrations. With this work we wanted to complete the Raman scattering investigations conducted on heavily doped *p*-type GaAs during the past few years aimed at elucidating the electron (hole)-phonon interaction. The results of such studies concerning the TO phonon electronic-continuum interaction[5,6] and about this continuum itself have already been published.[7] We have performed Raman scattering experiments from (100) faces in backscattering geometry. For this orientation of the sample surfaces, Raman scattering from LO-like modes is allowed while TO scattering should be forbidden. The first-order Raman spectra from surfaces under consideration display, for all the samples investigated, two kinds of lines. One of these lines behaves as scattering by longitudinal-optical modes. With increasing free-hole concentration this LO-like line shifts from the LO phonon frequency to lower frequencies. This line corresponds to coupled LO-phonon–plasmon modes with wave vectors much larger than those given by the nominal $\vec{q}$ transfer of the photons. We conjecture that the wave-vector nonconservation arises from elastic scattering by the ionized acceptor impurities. For the discussion of the shifts, broadening, and intensities of the LO-like line as a function of hole concentration we shall consider phenomenologically the wave-vector nonconservation and how it affects the line shapes of the coupled modes. We were not able to observe the long-wavelength $L^\pm$ modes in *p*-type GaAs even for allowed scattering geometry and with incident photons away from resonance. Even in this case we observed LO-like modes which resemble those measured in forbidden configuration and under resonant conditions.[13]

The other lines observed in the Stokes-Raman spectra seem to correspond to scattering by transverse-optical phonons in spite of the fact that such scattering is forbidden by the selection rules for (100) surfaces. Together with the Raman scattering by the coupled longitudinal modes, we report in this paper the observation of forbidden TO-phonon Raman scattering which is induced by wave-vector nonconservation brought about in the Raman process by the presence of impurities. The forbidden TO Raman lines display self-energy effects which we can explain with the $\vec{q}$ nonconservation mechanism postulated for the LO-like modes.

The organization of the paper is as follows: The experimental details will be given in the next section. The results and discussions are presented in Sec. III. In the first part of the discussions the

LO-like modes are considered. The forbidden TO scattering is discussed in the second part of Sec. III. Finally, the Appendix gives a brief description of how to calculate the observed self-energy effects of the TO phonons.

II. EXPERIMENTAL DETAILS

The GaAs samples were cut from Zn-doped single crystals and their hole concentrations determined by means of Hall-effect measurements. Surfaces with a (100) orientation, polished and etched with an aqueous solution of NaOCl, were used in the experiment. The samples were glued with silver paste to a copper cold finger which was placed in an evacuated glass Dewar and maintained in contact with a liquid-nitrogen bath.

The Raman measurements were performed in the standard backscattering geometry. The spectra were excited with either the 5145 Å (2.41 eV) or the 4579 Å (2.71 eV) lines of an Ar^+-ion laser. The incident light was focused on the surface of the sample with a cylindrical lens in order to avoid heating. The scattered light was analyzed with a Jarrell-Ash 1-m double monochromator equipped with holographic gratings and detected with an RCA 31034 photomultiplier with photon counting electronics. The counts were stored in a multichannel analyzer with typical integration times ranging from 2 to 10 s and a spacing of ~ 1 cm^{-1} between adjacent channels. The wave-number scale was carefully calibrated by using different lines of a low-pressure Ne lamp. The calibration procedure was repeated twice a day to take care of temperature drift.

III. RESULTS AND DISCUSSIONS

Figures 1 and 2 display typical Stokes-Raman spectra recorded at $T=77$ K from (100) surfaces in the energy range between 240 and 330 cm^{-1} for a series of hole concentrations. The different scattering configurations are indicated, where $x=[100]$, $y=[010]$, and $z=[001]$. In general, two Raman lines are observed: One line peaks at around 295 cm^{-1} for samples of hole concentrations between 10^{17} to 10^{18} holes cm^{-3} and shifts to lower energies with increaisng hole concentrations while the other line peaks around 271 cm^{-1} for almost all hole concentrations. From the well-known frequencies of the optical modes of undoped GaAs it is easy to establish that the lines peaking at 271 cm^{-1} correspond to scattering by transverse-optical phonons (TO phonons).[6] The other lines, lying at higher energies, arise from scattering by longitudinal-optical modes (LO modes).[13]

For display purposes the measured Raman spectra shown in Figs. 1 and 2 were normalized with different constants. Therefore, a direct comparison between the intensities of the Raman lines in these figures is not possible. However, all the experimental information about the dependence of intensities on hole concentration, linewidth, and peak positions of the TO- and LO-like Raman lines is displayed in Figs. 3–8. In Table I the notations we have chosen to represent the different scattering geometries are summarized together with the selection rules for first-order Raman scattering from (100) surfaces. The observed TO- and LO-like lines correspond to scattering by bulk modes. The penetration depth of the incoming photons varies approximately from 400 Å (for $\hbar\omega_L=2.71$ eV) to 800 Å (for $\hbar\omega_L=2.41$ eV), while the depth of the surface depletion layer is of the order of 200 Å for 10^{18} acceptors cm^{-3} and decreases with increasing acceptor concentration. On the other hand, we do not observe in our measurements with the heaviest doped samples the unscreened LO phonon of the depletion layer, which shows up when surface effects are dominant.

We discuss first the scattering due to the LO-like modes, which is allowed by the second-rank tensor selection rules quoted in Table I. As in the case of heavily doped n-type GaAs we expect for the long-wavelength ($\vec{q}\simeq 0$) coupled modes, a Raman line at the LO-phonon frequency (~ 295 cm^{-1}) for very low hole concentrations and a shift of this line (the $\vec{q}\simeq 0$ L^+ coupled mode) to higher energies when the hole concentration increases.[8,9] This behavior of the long-wavelength L^+ modes does not show up in our experiments. Instead a decrease of the LO-like Raman lines to lower energies with increasing hole concentration is seen (see Fig. 3). Together with the expected shifts of the L^+ modes, the $\vec{q}\simeq 0$ L^- modes should appear at very low frequencies for the samples with the lowest hole concentration and reach the TO phonon for the heaviest doped samples.[8,9] We did not observe any evidence of the long-wavelength L^- modes in the measured Stokes spectra of p-type GaAs. We shall come back to this point when we discuss the TO-like Raman lines.

The shifts of the LO-like Raman lines to lower energies with increaisng hole concentration (see

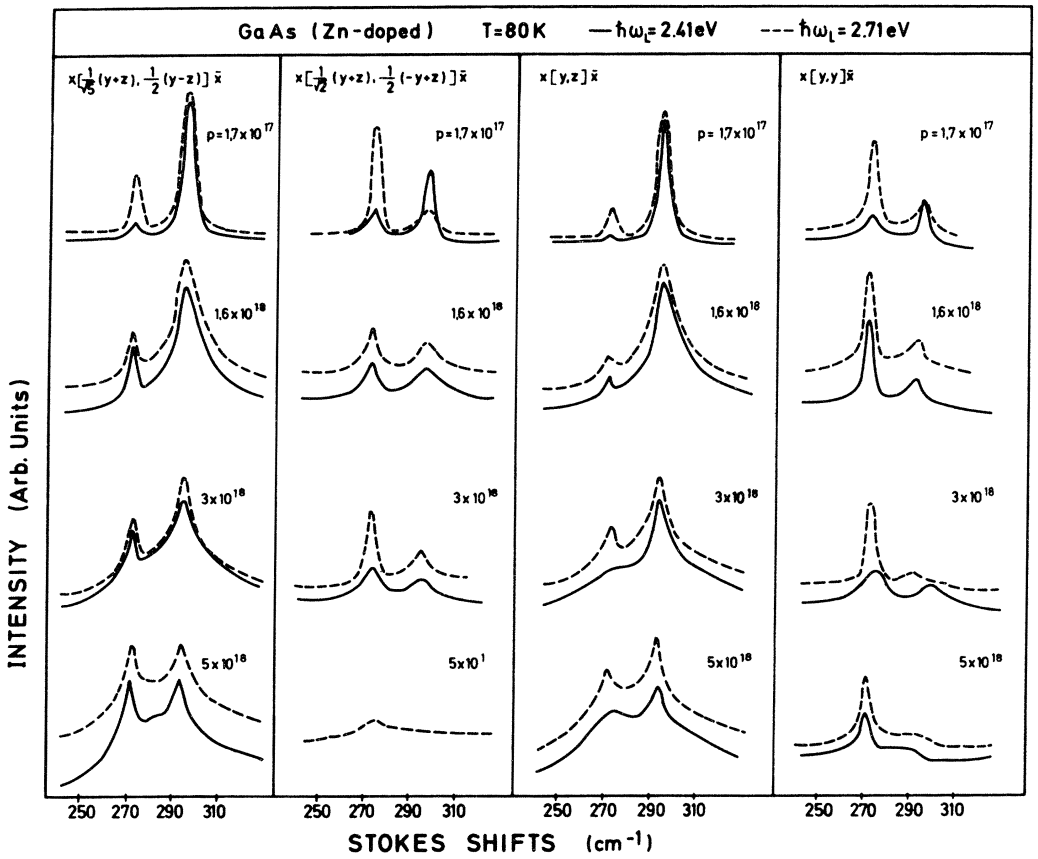

FIG. 1. First-order Stokes-Raman spectra from (100) surfaces of heavily doped p-type GaAs with hole concentrations ranging from 10^{17} to 5×10^{18} holes cm^{-3}. The spectra drawn with solid lines were taken with an incident photon energy of 2.41 eV while the dashed lines correspond to spectra excited with an incident photon energy of 2.71 eV. Standard notation is used to describe the scattering configurations, e.g., $x[y,z]\bar{x}$, where x and $\bar{x}$ are the incident and scattered wave vectors, y and z the incident and scattered electric field vectors. x,y,z are chosen as follows: $\vec{x}=(1,0,0)$, $\vec{y}=(0,1,0)$, and $\vec{z}=(0,0,1)$. Two different Raman lines can be distinguished: the line peaking around 271 cm^{-1}, very close to the transverse-optical phonons, and a second line at around 295 cm^{-1} (or slightly below) due to impurity-induced scattering by coupled LO-phonon—plasmon modes of large wave vector. Raman scattering by LO-like modes is allowed by the selection rules quoted in Table I, while scattering by TO modes is forbidden.

Figs. 1—3) correspond to the fact that we measure coupled modes (L^-) with average wave vectors much larger than the $\vec{q}$ transfer of the incident and scattered photons (see inset in Fig. 3). At low doping the "coupled mode" coincides with the LO frequency; at high doping we measure an average frequency of this coupled mode which lies slightly below LO. Raman scattering by coupled modes of large wave vectors has been observed in forbidden scattering geometry and with incident photons in resonance with the E_1 gap of GaAs.[13] It seems that the dominant process does not conserve wave vectors even in the allowed configuration and away from resonance. The wave-vector nonconservation is attributed to elastic scattering of the photoexcited electrons and holes by the ionized acceptor impurities.[15] Processes in which $\vec{q}$ is not conserved have been observed in many Raman and luminescence investigations of p-type GaAs (Refs. 6, 13, and 16) as well as in Raman and Brillouin studies performed on CdSe.[17]

The scattering efficiency of the LO-phonon—plasmon modes has a contribution due to their phonon component and another one due to the plasmon. The latter is of the charge-density—fluctuations type and contains interband (electro-

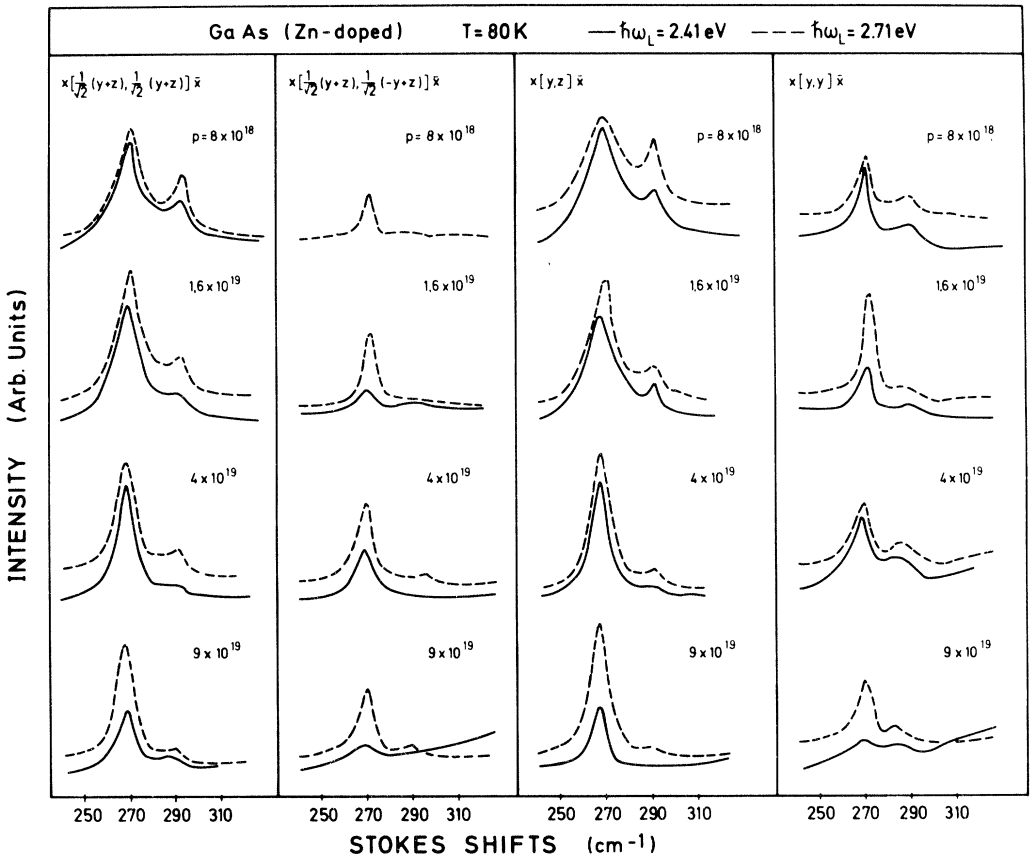

FIG. 2. First-order Stokes-Raman spectra from (100) surfaces of heavily doped p-type GaAs with hole concentrations ranging from 8×10^{18} to 10^{20} holes cm^{-3}. The spectra drawn with solid lines were taken with an incident photon energy of 2.41 eV while the dashed lines correspond to spectra excited with an incident photon energy of 2.71 eV. The notation for the scattering configuration is described in the caption of Fig. 1. The Raman lines lying in the high wavenumber side of the spectra arise from scattering by coupled LO-phonon—plasmon modes of large wave vectors. The Raman lines around 271 cm^{-1} for the samples with 8×10^{18} and 1.6×10^{19} holes cm^{-3} correspond to forbidden TO phonon scattering. For the samples with 4×10^{19} and 9×10^{19} holes cm^{-3} these lines are the completely screened LO phonon modes.

optic) and intraband terms.[8,9] The intraband contribution is significant only near direct resonant gaps which start or end at the positions of the free carriers in k space (E_0 and $E_0+\Delta_0$ gaps in the case of GaAs).[11] This is not the case in the experiments discussed here which involve only the E_1 and $E_1+\Delta_1$ resonances. The interband terms of the charge-density fluctuations can be estimated to be negligible with the known Faust-Henry coefficient.[8,9] We are thus left here with phonon contributions to the scattering efficiency. These, in turn, can be of two types: deformation potential and Fröhlich (for LO phonons), each of the intraband and interband variety.[14,18]

Near the E_1 gaps (two-dimensional critical points) the intraband deformation-potential contribution to the scattering efficiency of pure samples is of the form $|E_1-\hbar\omega|^{-2}$. The interband contribution, dominant near E_1, is of the form $|\ln|E_1-\hbar\omega||^2$ for $|E_1-\hbar\omega|<\Delta_1$ and for $|E_1-\hbar\omega|>\Delta_1$, a condition which holds in our experiments; it regains the same form as the intraband contributions (see Table II). Δ_1 is the spin-orbit splitting along the Λ direction.

In an undoped material the Fröhlich effects of LO phonons on valence and conduction bands cancel to first order, leaving only a forbidden $\vec{q}$-dependent term which contributes a resonance like

TABLE I. Scattering configurations measured in our experiments and notations adopted to display the results in Figs. 3–8, together with the selection rules for first-order Raman scattering by optical phonons and coupled modes. The mechanisms involved in the light scattering by coupled modes are also quoted.

Scattering configuration[a]	Notation adopted $\hbar\omega_L=2.41$ eV	$\hbar\omega_L=2.71$ eV	Selection rules for first-order Raman scattering assuming wave-vector conservation[b]	Selection rules for longitudinal-coupled modes and scattering mechanisms involved[c]
$x[1/\sqrt{2}(y+z),1/\sqrt{2}(y+z)]\bar{x}$	□	■	LO-allowed TO-forbidden	Allowed deformation potential, electro-optic charge-density fluctuations, and impurity-induced Fröhlich interaction
$x[1/\sqrt{2}(y+z),1/\sqrt{2}(-y+z)]\bar{x}$	Δ	▲	LO-forbidden TO-forbidden	Forbidden
$x(y,y)\bar{x}$	◇	◆	LO-forbidden TO-forbidden	Allowed charge-density fluctuations and impurity-induced Fröhlich interaction
$x(y,z)\bar{x}$	○	●	LO-allowed TO-forbidden	Allowed deformation-potential and electro-optic

[a] x and $\bar{x}$ are the directions of incident and scattered wave vectors, y and z the incident and scattered electric fields. $\vec{x}=(1,0,0)$, $\vec{y}=(0,1,0)$, and $\vec{z}=(0,0,1)$.
[b] Reference 14.
[c] Reference 8.

$|E_1-\hbar\omega|^{-4}$ to the scattering efficiency. For doped materials an intraband Fröhlich charge-density–fluctuation term appears. As for the plasmons mentioned above, it is zero only if effects of the $E_1-E_1+\Delta_1$ gaps are treated. Another way of lifting the conduction-valence Fröhlich cancellation is through elastic scattering by the impurities.[13,15] The corresponding scattering potentials have opposite signs for electrons and holes and the total scattering matrix element depends on the square of the carrier charge: The effects of the conduction and the valence bands thus now add instead of canceling. However, the resonance should contain an extra energy denominator due to the additional impurity potential perturbation (scattering efficiency $\sim|E_1-\hbar\omega|^{-4}$). The electro-optic *interband* Fröhlich term of the phonons will also be neglected.

Likewise one can have impurity-induced intraband deformation-potential terms (scattering efficiency $\sim|E_1-\hbar\omega|^{-4}$) and interband terms (scattering efficiency $\sim|E_1-\hbar\omega|^{-4}$). All the cases of relevance here (intraband for $|E_1-\hbar\omega|>\Delta_1$ and impurity-induced Fröhlich) resonate like $|E_1-\hbar\omega|^{-4}$. Table II summarizes the resonant behaviors of the scattering efficiency discussed above.

The efficiency for light scattering by the coupled modes of a given wave vector $\vec{q}$ due to the deformation-potential mechanism (DP in what follows) is given by

$$\frac{\partial^2 R(\vec{q})}{\partial\Omega\partial\omega}\propto-\frac{(\omega_0^2-\omega^2)^2}{(\omega_{\mathrm{TO}}^2-\omega^2)^2}\,\mathrm{Im}\frac{1}{\epsilon(\vec{q},\omega)} \tag{1}$$

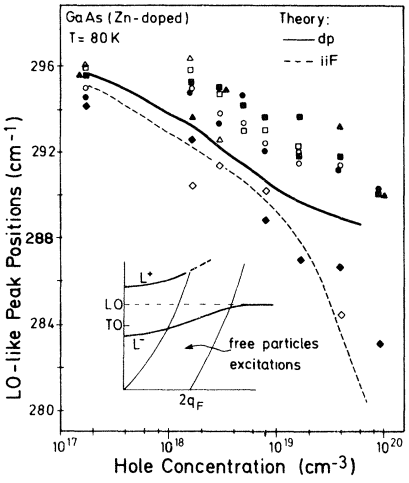

FIG. 3. Hole-concentration dependence of the peak positions of the LO-like Raman lines. The notation used is explained in Table I. The LO-like Raman lines shift to lower energies with increasing hole concentration. The shifts are more pronounced for the lines due to the impurity induced Fröhlich mechanism. The solid and dashed lines display the results of the theoretical calculations for an incident photon energy of 2.71 eV.

multiplied by the appropriate resonance factor described above and in Table II. In Eq. (1) $\omega_{TO}=271.5\ \text{cm}^{-1}$ is the transverse-optical phonon frequency and $\omega_0=\omega_{TO}(1+C)^{1/2}=180\ \text{cm}^{-1}$, with C the Faust-Henry coefficient. The total dielectric constant can be written in the following way:

$$\epsilon(\vec{q},\omega)=\epsilon_\infty\frac{\omega_{LO}^2-\omega^2}{\omega_{TO}^2-\omega^2}+4\pi\chi_{fh}(\vec{q},\omega)\ , \tag{2}$$

where $\omega_{LO}=295.5\ \text{cm}^{-1}$ is the longitudinal-optical frequency and $\chi_{fh}(\vec{q},\omega)$ the susceptibility of the free holes at the frequency ω and wave vector $\vec{q}$. $\epsilon_\infty=11.1$ corresponds to the high-frequency dielectric constant of GaAs at frequencies well below the optical gap. When wave-vector nonconservation takes place, the efficiency of the light scattering due to the DP mechanisms can be represented by

$$\frac{\partial^2 R}{\partial\Omega\partial\omega}\propto\int f(\vec{q})g(\vec{q})\frac{\partial^2 R^{(q)}}{\partial\omega\partial\Omega}d\vec{q} \tag{3}$$

with the functions $f(\vec{q})$ and $g(\vec{q})$ accounting, respectively, for some weighting in the relative contributions of the different phonon wave vectors participating in the total scattering process and the resonant enhancement of the scattering efficiency as the photon energy of the incoming photons approaches some direct energy gap of the material.

We attribute the nonconservation of the wave vectors to elastic scattering of the photocreated carriers by the ionized acceptor impurities.[15] The potential of one isolated impurity is approximated by

$$V(r)=\frac{1}{r}e^{-q_{TF}r}\ , \tag{4}$$

with $\vec{q}_{TF}$ the Thomas-Fermi wave vector taking into account the screening of the potential due to the presence of the free carriers. We use as a weighting function for the different wave vectors

TABLE II. Resonant behavior of the Raman scattering efficiency near the E_1 and $E_1+\Delta_1$ energy gaps.

Process	Undoped samples	Impurity induced
Deformation potential: interband[a]	$\lvert\ln\lvert E_1-\hbar\omega\rvert\rvert^2$	$\lvert E_1-\hbar\omega\rvert^{-2}$
Deformation potential: intraband and interband[b]	$\lvert E_1-\hbar\omega\rvert^{-2}$	$\lvert E_1-\hbar\omega\rvert^{-4}$
Fröhlich	$\lvert E_1-\hbar\omega\rvert^{-4}$	$\lvert E_1-\hbar\omega\rvert^{-4}$
Charge-density fluctuations	0	0

[a]Holds for $\lvert E_1-\hbar\omega\rvert<\Delta_1$.
[b]Holds for $\lvert E_1-\hbar\omega\rvert>\Delta_1$.

participating in the Raman scattering process the square of the Fourier transform of the impurity potential (this procedure is correct except in the high-impurity concentration limit). The function $f(\vec{q})$ in Eq. (3) will thus be replaced by

$$f(\vec{q})=\left[\frac{4\pi}{q^2+q_{\mathrm{TF}}^2}\right]^2 . \tag{5}$$

To excite the Raman spectra we used the 2.41- and 2.71-eV lines of an Ar^+-ion laser. At these energies the resonance of the E_0 and $E_0+\Delta_0$ gaps have completely died out.[18] The energies of the incoming photons lie, however, sufficiently near the E_1 gap of GaAs (~ 3 eV) for resonance effects to appear, especially at 2.71 eV. To consider the enhancement of the Raman efficiency when the laser line goes from the green (2.41 eV) to the blue (2.71 eV), we use for the function $g(\vec{q})$ in Eq. (3) the following expression:

$$g(\vec{q})=\left[\frac{1}{E_1+\frac{\hbar^2q^2}{2M^*}-\hbar\omega_L}\right]^2\left[\frac{1}{E_1-\hbar\omega_L}\right]^2 . \tag{6}$$

Equation (6) is equivalent to the results of Table II except that the large wave-vector transfer for one of the intermediate states has been included in the corresponding energy denominators. $\hbar\omega_L$ represents the incident photon energy and $h^2q^2/2M^*$ the increase of the effective gap in the resonant Raman process for phonons or coupled modes of finite wave vectors. M^* stands for the center-of-mass exciton mass near the E_1 gap: $M^*=M_e^*+M_h^*$ with $M_e^*(M_h^*)$ the effective electron (hole) effective mass at the E_1 gap. We note that the square of the scattering probability amplitude appears in Eqs. (5) and (6).[19] Inserting Eqs. (1), (5), and (6) into Eq. (3) and performing the angular integration, the efficiency of the light scattering by coupled modes due to the DP mechanism is

$$\frac{\partial^2R}{\partial\Omega\partial\omega}\propto-\left[\frac{1}{E_1-\hbar\omega_L}\right]^2\frac{(\omega_0^2-\omega^2)^2}{(\omega_{\mathrm{TO}}^2-\omega^2)^2}\int_0^\infty\left[\frac{1}{q^2+q_{\mathrm{TF}}^2}\right]^2\left[\frac{1}{E_1+(\hbar^2q^2/2M^*)-\hbar\omega_L}\right]^2 q^2\,\mathrm{Im}\frac{1}{\epsilon(q,\omega)}dq . \tag{7}$$

The other mechanism responsible for the light scattering by the coupled modes is the impurity-induced Fröhlich mechanism (IIF in what follows) for which[13]

$$\frac{\partial^2R(\vec{q})}{\partial\Omega\partial\omega}\propto-f(\vec{q})g(\vec{q})\,\mathrm{Im}\frac{1}{\epsilon(\vec{q},\omega)} . \tag{8}$$

Although listed as allowed for parallel incident and scattered polarizations in Table I, Raman scattering by the IIF mechanism is of a *forbidden* nature: It corresponds to $\vec{q}$-dependent Raman tensors.[13,14,18] With the wave-vector nonconservation produced by the impurity scattering the product of the functions $f(\vec{q})g(\vec{q})$ can be written for two-band Fröhlich processes as follows:

$$f(\vec{q})g(\vec{q})=\left[\frac{1}{q}\left[\frac{1}{E_1+(\hbar^2q^2/2M_e^*)-\hbar\omega_L}+\frac{1}{E_1+(\hbar^2q^2/2M_h^*)-\hbar\omega_L}\right]\frac{1}{q^2+q_{\mathrm{TF}}^2}\right]^2\left[\frac{1}{E_1-\hbar\omega_L}\right]^2 . \tag{9}$$

The factor q^{-1} comes from the Fröhlich electron-phonon coupling and the positive sign in the expression within the brackets describes the different signs of the interactions of electron impurity and hole impurity. Inserting Eqs. (8) and (9) in a type of expression given by Eq. (3) and performing the angular integration, one gets the equivalent of Eq. (7) for the case of the IIF mechanism:

$$\frac{\partial^2R}{\partial\Omega\partial\omega}\propto-\left[\frac{1}{E_1-h\omega_L}\right]^2\int_0^\infty\left[\frac{1}{E_1+(\hbar^2q^2/2M_e^*)-\hbar\omega_L}+\frac{1}{E_1(\hbar^2q^2/2M_h^*)-\hbar\omega_L}\right]^2 \times\left[\frac{1}{q^2+q_{\mathrm{TF}}^2}\right]^2\mathrm{Im}\frac{1}{\epsilon(q,\omega)}dq . \tag{10}$$

With Eqs. (7) and (10) we expect to describe the hole concentration dependence of the shifts and linewidths of the LO-like Raman lines. In the case of the scattering configuration $x[1/\sqrt{2}(y+z), 1/\sqrt{2}(y+z)]\bar{x}$, the scattering by the IIF mechanism will be neglected in comparison with

that of the DP mechanisms, due to the "forbidden nature" of the first process. In the evaluation of Eqs. (7) and (10) we use the Lindhard expression for the contribution of the free holes to the total dielectric constant [Eq. (2)] and assume that the free holes are all in the heavy-hole valence band (i.e., we neglect the small amount of light holes). The following effective masses were used in the calculations: For the heavy holes near the Γ point $m^*_{hh}=0.62$,[20] for the electron and hole near the E_1 gap $M^*_e=0.11$ (Ref. 21) and $M^*_h=2M_e$.[21] The E_1 energy gap was set equal to 3 eV.[18,21] The other parameters needed for the evaluation of the susceptibility of the free holes are listed in Table III. Computer calculations of the scattering efficiencies as given by Eqs. (7) and (10) were performed as a function of ω. From the results, a graphical determination of the theoretical peak positions and widths of the LO-like Raman modes was made.

Figure 3 displays calculated and observed shifts of the LO-like Raman lines with increasing hole concentration. For a given hole concentration the Raman lines corresponding to the IIF mechanisms are observed at lower energies than the lines due to the DP mechanisms. The solid and dashed lines represent the calculated peak positions for an incident photon energy of 2.71 eV. The experimental trends for the different scattering mechanisms are reproduced by the calculation. The larger shifts of the Raman lines of the coupled modes by the IIF are a result of the fact that the functions which multiply the imaginary part of ϵ^{-1} weigh strongly the smaller $\vec{q}$ vectors. Consequently, L^- modes of lower frequencies are more probable in the IIF mechanism as compared with those participating in the DP scattering (see inset in this figure).

Figure 4 shows the hole-concentration dependence of the linewidths of the LO-like Raman spectra of Figs. 1 and 2. For the DP mechanisms an increase of the linewidth with increasing hole concentration takes place. For concentrations higher than 5×10^{18} holes cm^{-3} the linewidths seem to become smaller. The linewidths of the coupled modes due to the IIF mechanisms apparently increase monotonically with hole concentration, although the experimental scatter is very large. The experimental behavior just mentioned agrees with the hole concentration dependence of the broadening of the LO-like lines measured in forbidden scattering geometries and resonant incident photon energy.[13] The lines drawn in Fig. 4 give the results of our calculations for an incident photon energy of 2.71 eV. The observed hole-concentration dependence of the broadenings is qualitatively reproduced by the theory. The same kind of analysis carried out to explain the different behavior of the shifts for a given hole concentration and different scattering mechanisms can be made for the broadenings. The width of the LO-like Raman lines is proportional to the imaginary part of the free-hole susceptibility. When the LO frequency lies within the free-particle excitation spectrum the imaginary part of the susceptibility is very large for wave vectors much smaller than the Fermi wave vector $\vec{q}_F$. When the wave vectors become larger than $\vec{q}_F$ a strong decrease of the imaginary part of the susceptibility takes place.[22] The weighting factors for the wave vectors in the Raman efficiency of the DP mechanisms allow scattering by modes of wave vectors larger than the

TABLE III. Parameters used to evaluate the Lindhard free-hole susceptibility. The last column includes the wave vector for which the function which multiplies the imaginary part of ϵ^{-1} in Eq. (7) has its maximum.

Free-hole concentration (10^{18} cm^{-1})	Fermi energy E_F (cm^{-1})	Fermi wave vector q_F [10^6 cm^{-1}]	Thomas-Fermi wave vector q_{TF} [10^6 cm^{-1}]	q_{max}/q_F
90	990	13.9	13.4	0.4
40	576	10.6	11.7	0.5
16	312	7.8	10	0.64
7	180	5.9	8.7	0.79
5	143	5.2	8.3	0.88
3	102	4.5	7.6	1
1.6	67	3.6	6.9	1.14
0.17	15	1.7	4.7	1.92

Fermi wave vector $\vec{q}_F$, while, on the other hand, wave vectors near zero are stronger weighted in the case of the IIF mechanism. This fact and the described behavior of the imaginary part of the free-hole susceptibility can explain why the LO-like lines for the IIF mechanism are wider than those of the DP ones in the heaviest doped samples, as the IIF mechanism samples regions where the imaginary part of the susceptibility is very large.

At this point we would like to discuss the possible reasons why the long-wavelength L^+ and L^- modes are not seen in our experiment. In the description of the coupled modes for $\vec{q}\simeq 0$ it is common to write a Drude-type susceptibility for the free carriers with a phenomenological parameter accounting for broadening effects within the free-carrier system.[8] This parameter can be related to the lifetime of the free carriers as obtained from the mobility. In the case of p-type GaAs we expect to observe the strong coupling of the $\vec{q}\simeq 0$ LO phonons and plasmons (the $\vec{q}\simeq 0$ $L^{\pm}$ modes) and the shifts of these modes for a hole concentration ranging from 10^{18} to 10^{19} holes cm^{-3}. However, from mobility data for samples with hole concentrations within this range we estimate that the phenomenological broadening should be comparable with the plasma frequency. This fact "decouples" the $\vec{q}\simeq 0$ LO phonons and plasmons. On the other hand, assuming wave-vector nonconservation (which allows to explain both the LO-like and TO-like Raman lines), we see from Eq. (7) for the DP mechanism (the stronger one for the incident photon energies used in the experiment) that the density of states for coupled modes of very short wave vectors is negligible. Therefore, Raman scattering by those modes is less probable than scattering by modes of larger wave vectors.

To conclude the discussion of the LO-like modes we consider now the dependence of the intensities of these lines on hole concentration. Figure 5 gives the integrated intensities, that is, the area under the experimental spectra, as a function of the hole concentration. Two different types of behavior are distinguished: The intensity of the lines due to the DP mechanisms shows an increase for intermediate hole concentrations with a remarkable decrease for concentrations above 10^{19} holes cm^{-3}. The intensities of the LO-like lines due to the IIF mechanisms do not depend strongly on hole concentration. By comparing the intensities for the DP mechanisms with those of IIF, the forbidden nature of the LO-like Raman lines due to the latter mechanism is confirmed: It is thus justified to have neglected the IIF in the scattering geometry $x[1/\sqrt{2}(y+z),1/\sqrt{2}(y+z)]\bar{x}$, where the two scattering mechanisms are present together (see Table I). Some residual completely forbidden LO-like Raman lines were observed in the configuration

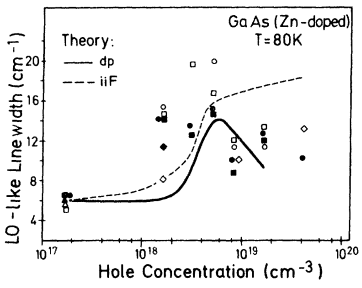

FIG. 4. Hole-concentration dependence of the linewidth of the LO-like Raman lines. The notation used is explained in Table I. After an initial increase with increasing hole concentrations (up to 5×10^{18} holes cm^{-3}) the linewidths of the LO-like lines due to the DP mechanisms decrease for very large hole concentrations. The linewidths for the IIF mechanisms seem to increase monotonically with increasing hole concentrations. The solid and dashed lines represent the theoretical calculations of the linewidths for an incident photon energy of 2.71 eV.

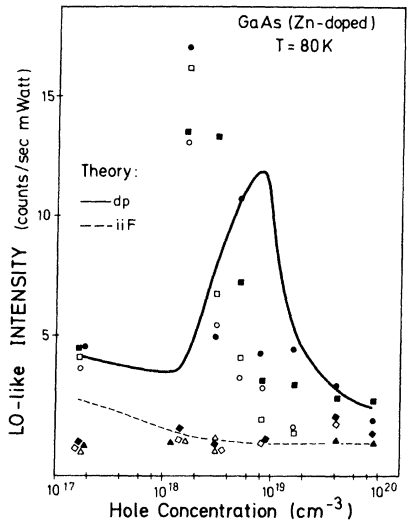

FIG. 5. Hole-concentration dependence of the intensities of the LO-like lines. The notation is explained in Table I. The intensities for the DP mechanisms are much larger than those for the IIF mechanism, a fact which confirms the forbidden nature of the latter process. The solid and dashed lines give the calculated intensities for an incident photon energy of 2.71 eV.

$x[1/\sqrt{2}(y+z), 1/\sqrt{2}(-y+z)]\bar{x}$ (see Table I). The origin of these lines can be attributed to slight misorientations of the sample surfaces or to surface irregularities due to the polishing-etching procedure.

A theoretical estimate of the intensities can be made by calculating the following integral:

$$I_{\mathrm{LO}} \propto N \int \frac{\partial^2 R}{\partial\Omega\partial\omega} d\omega \tag{11}$$

with the scattering efficiency $\partial^2 R/\partial\Omega\partial\omega$ given by Eqs. (7) and (10). N is the acceptor concentration taken equal to the free-hole concentration. The lines drawn in Fig. 5 represent the calculated intensities for an incident photon energy of 2.71 eV. The intensities of the sample with 1.7×10^{17} holes cm^{-3} were the only adjustable parameters. They were fixed to the values shown in Fig. 5. As seen in this figure, qualitative agreement of the calculation with the experiment is achieved in the case of the intensities of the LO-like lines, both for the DP and the IIF cases.

In the second part of this section we want to discuss the behavior of the Raman lines peaking around 271 cm^{-1} in the spectra displayed in Figs. 1 and 2. These lines arise from scattering by transverse-optical phonons (TO phonons). First-order Raman scattering from (100) surfaces by $\vec{q}\simeq 0$ TO phonons is forbidden in backscattering geometry as indicated in Table I. However TO-phonon Raman scattering has been reported several times in experiments dealing with (100) faces, particularly in heavily doped materials.[12,23] The appearance of these lines was always attributed to misorientation of the surfaces. We have performed a detailed study of the TO lines displayed in Figs. 1 and 2 as a function of the hole concentration covering a range from 10^{17} to 10^{20} holes cm^{-3}. The TO line is present for all the samples. Its linewidth and intensity show an interesting and systematic behavior which excludes misorientation of the (100) surfaces used in the experiment as the main cause for the violation of the selection rule for TO scattering.

Our interpretation of the origin of the forbidden TO Raman scattering can be summarized as follows: According to the irreducible components of the Raman tensor and the polarization of the incoming and outgoing photons, an optical phonon is created in the first-order Raman process. If the wave vector of the created phonon is given by the $\vec{q}$ transfer of the light, then the polarization of this phonon with respect to $\vec{q}$ is fixed by the irreducible components of the Raman tensor. However, when wave-vector nonconservation takes place, this is no more the case. We believe that the TO Raman lines observed for all the samples measured correspond to forbidden TO scattering (in the sense of the selection rules quote in Table I) which becomes allowed because of the wave-vector nonconservation. The DP and IIF mechanisms discussed previously for LO-like modes are also responsible for the creation in the Raman process of a phonon which becomes transverse due to the change of the wave vector with respect to the polarization produced by the impurity scattering.

We consider now the hole-concentration dependence of the properties of these TO lines. Figure 6 reproduces the peak positions of the lines as a function of the hole concentration. Up to 10^{19} holes cm^{-3} within the experimental error no shifts are observed with respect to the TO frequency of pure GaAs ($\sim$271.5 cm^{-1}). For the samples with 4×10^{19} and 9×10^{19} holes cm^{-3} clear shifts to lower energies are measured.

The linewidths of the TO Raman spectra which are displayed in Fig. 7 show different behavior as a function of the hole concentration depending on the polarization of the incident and scattered pho-

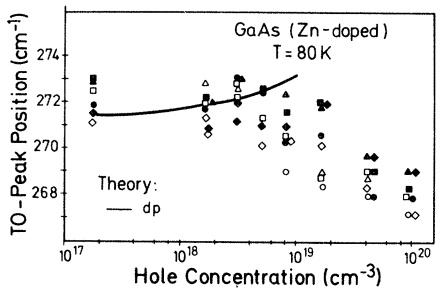

FIG. 6. Dependence of the peak positions of the TO-like phonon Raman lines on hole concentration. The notation used is that of Table I. A clear shift of these lines to lower wave numbers is measured for the samples with 4×10^{19} and 9×10^{19} holes cm^{-3}. The TO-like Raman lines for these hole concentrations correspond to the completely screened LO phonons. They shift to lower energies due to the interaction with the Raman-active intra-valence-band continuum reported in Ref. 7. The TO lines for the samples with lower hole concentrations correspond to impurity-induced forbidden scattering by TO phonons discussed in the text. The solid line gives the calculated peak positions evaluated with the equations in the Appendix for decay of the TO phonons into free-particle excitations within the heavy-hole valence band.

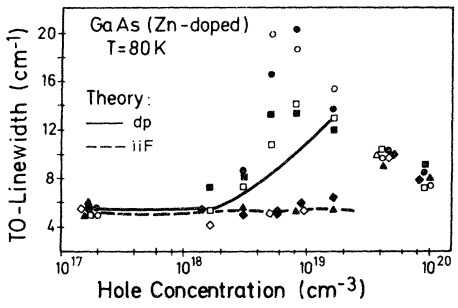

FIG. 7. Hole-concentration dependence of the linewidth of the TO-like Raman lines. The notation used is explained in Table I. The linewidths of the samples with 4×10^{19} and 9×10^{19} holes cm^{-3} do not depend on the scattering configuration. The broadening of these lines over the natural linewidth arises from the same interaction which gives place to the shifts displayed in Fig. 6. For samples of lower hole concentrations the linewidths of the forbidden TO lines depend on the scattering mechanisms involved in the Raman process. A broadening is measured with increasing hole concentration for the lines due to the DP mechanisms. The natural TO linewidth is measured in the case of the IIF mechanisms. The solid and dashed lines display the linewidths calculated with the equations in the Appendix for decay of the TO phonons into free-particle excitation spectrum within the heavy-hole valence band.

tons. For the phonons created through the DP mechanisms an increase of the linewidths with increasing hole concentration takes place, while the phonons created by the IIF mechanisms do not broaden. Again an exception are the TO lines corresponding to the samples with 4×10^{19} and 9×10^{19} holes cm^{-3}, for which the linewidths do not depend on the mechanisms involved.

The different behaviors in the shifts as well as in the broadening of the TO lines for samples of these two concentrations can be explained by considering that these lines are the L^- modes corresponding to the completely screened LO phonons. For very large hole concentrations ($\omega_p >> \omega_{LO}$) the screened LO phonons are almost dispersionless up to wave vectors well inside the free-particle excitation spectrum, so that the characterization of these lines as L^- modes does not invalidate our assumption of $\vec{q}$ nonconservation. In the discussion of the intensities of the TO lines we will see that $\vec{q}$ nonconserving processes must also be present in the scattering by the screened LO modes.

A very interesting point is that the peaks due to completely screened LO modes show the same self-energy effects seen for the TO phonons: A shift of about 2 cm^{-1} to lower energies and a broadening of the same magnitude were measured for the TO phonons of the heaviest doped p-type GaAs samples in Raman-allowed configurations.[5,6] These self-energy effects are the result of a deformation-potential-type interaction between the TO phonon (or in this case the completeley screened LO phonon) and a Raman-active continuum of indirect transitions within the heavy-hole valence band.[7] Due to the indirect transition nature of the electronic continuum, a quantitative description of the self-energy of the screened LO modes is very difficult to perform.[6]

Having characterized the TO-like Raman lines of the heaviest doped samples we concentrate our attention now on the forbidden TO scattering of the samples with concentration lower than 4×10^{19} holes cm^{-3}. We consider first the hole-concentration dependence of the broadening shown in Fig. 7 for the TO-like lines under the assumption that they correspond to DP mechanisms. Because of the $\vec{q}$ nonconservation the wave vectors of the TO lines will be weighted by the function $q^2 f(\vec{q}) g(\vec{q})$. After they are created, the TO phonons interact with the holes decaying into the free-particle excitation within the heavy-hole band (the presence of some free holes in the light-hole valence band will be again neglected). This hole-phonon interaction gives place to changes in the phonon self-energy which are of a dispersive nature in the sense that they depend strongly on the wave vectors of the phonon. For heavily doped p-type Ge, $\vec{q}$-dependent self-energy effects have been studied theoretically[24] and experimentally verified.[6] An even more striking confirmation of this effect has been recently obtained by means of inelastic neutron scattering for acoustic phonons in n- and p-type Si.[25] The function $q^2 f(\vec{q}) g(\vec{q})$ with $f(\vec{q})$ and $g(\vec{q})$ given by Eqs. (5) and (6) has a pronounced maximum for the values of $\vec{q}$ listed in the last column of Table III. Assuming that the TO phonons created through the DP mechanisms have predominantly wave vectors for which $q^2 f(\vec{q}) g(\vec{q})$ is maximum and after being created, they decay in intraband hole excitations, it is possible to evaluate changes in the phonon self-energy. The details of the calculation are summarized in the Appendix. The solid line of Fig. 7 represents the broadenings calculated with Eq. (A3) without any adjustable parameter. The increase of the linewidths for the DP mechanisms with increasing hole concentration is reproduced by the calculation and corresponds to the

imaginary part of the self-energy of the phonons with $q = q_{max}$. For the IIF mechanism the maximum of the function which gives the wave-vector distribution in Eq. (10) takes place at $\vec{q} \simeq 0$. For small wave vectors $\hbar\omega_{TO}$ lies well above the free-particle excitation spectrum and the density of states at the phonon frequency is zero independently of the hole concentration (see Appendix). Therefore, the calculated additional broadening is zero for all hole concentrations (dashed line in Fig. 7), in agreement with the experiment. Hence for the IIF mechanisms the natural linewidth is measured.

We come back to the hole-concentration dependence of the peak positions of the TO lines shown in Fig. 6. In the case of the DP mechanisms the measured self-energy effects in the lifetime of the TO phonons (broadening of the Raman lines) should be accompanied by renormalizations of the phonon frequencies (shifts of the Raman lines). Within the model developed we can calculate the expected shifts by performing an evaluation of the integral (A1) with the expressions for the density of states as given in the Appendix. The hole-concentration dependence of the calculated shifts is shown by the solid line in Fig. 6. For samples with concentrations above 5×10^{18} holes cm^{-3} a slight shift to higher energies is calculated (this shift represents the decrease in self-energy with increasing $\vec{q}$). The calculated shifts, however, lie within the experimental uncertainty and are not observed. It turns out from the calculations with Eq. (A1) that a compensation takes place between the shifts due to the states below the TO frequency and those above this frequency. This fact can explain why strong self-energy effects are measured for the broadenings while none are observed for the shifts for concentrations below 10^{19} cm^{-3}.

The last point we want to discuss is the hole-concentration dependence of the intensities of the TO-like Raman lines as shown in Fig. 8. With increasing hole concentration the intensities of the TO-like lines due to the DP mechanisms are larger than those of the lines corresponding to the IIF mechanism. As in the case of the LO-like lines (Fig. 5) some residual scattering is observed in the geometry $x[1/\sqrt{2}(y+z), 1/\sqrt{2}(-y+z)]\bar{x}$, in which the creation of a phonon excitation is completely forbidden (see Table I). Also in Fig. 8 a comparison is made between the intensities of the TO-like Raman lines of the doped samples and the LO-phonon Raman line of very pure GaAs with carrier concentration lower than 10^{14} electrons cm^{-3}. The point displayed for the pure sample was measured for $\hbar\omega_L = 2.41$ eV in the $x[1/\sqrt{2}(y+z), 1/\sqrt{2}(y+z)]\bar{x}$ scattering geometry. As was discussed previously the Raman lines measured from (100) surfaces near the TO phonon frequency in the samples with concentrations above 4×10^{19} holes cm^{-3} correspond to the completely screened LO phonons. The intensities of these modes for the DP mechanisms should be smaller than the LO phonon intensity in pure GaAs if wave-vector conservation holds as the electro-optic scattering mechanism is completely screened for these concentrations. However, that is not the case as a consequence of the wave-vector nonconservation.

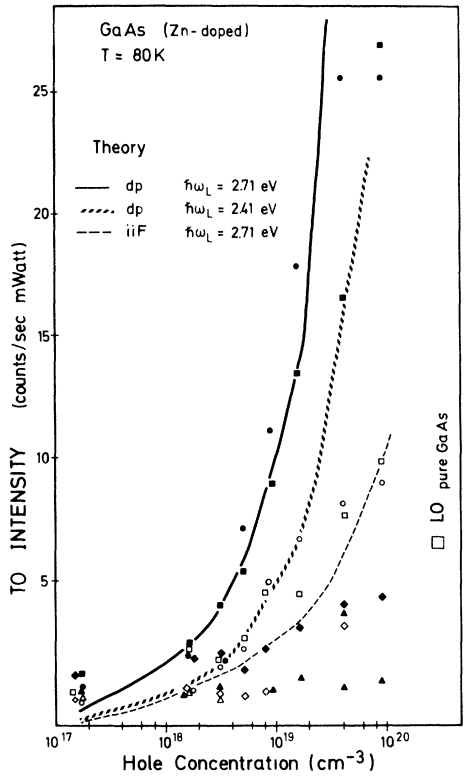

FIG. 8. Dependence of the intensities of the TO Raman lines on hole concentration. The notation used is that of Table I. The intensities of the TO lines due to the DP mechanisms are larger than those of the IIF mechanism. A resonant enhancement of the intensities takes place for the DP case when the incident photons approach the E_1 gap. The lines represent the intensities calculated with Eq. (12).

From this comparison we obtain one more argument for the validity of the interpretation that $\vec{q}$

nonconserving processes dominate the Raman scattering from p-type GaAs. For carrier concentrations between 3×10^{18} and 10^{19} holes cm^{-3} the TO-like lines display the same preresonant behavior of the E_1 gap as measured for the TO and LO Raman lines of pure GaAs (Refs. 18 and 26): The intensities of the lines excited with photons of 2.71 eV are larger than those excited with 2.41 eV. The intensities of the TO-like lines due to the IIF mechanisms are for all hole concentrations smaller than the LO intensity of the pure sample due to the forbidden nature of this mechanism. The IIF scattering is expected to be strongly enhanced only for laser photons exactly at the E_1 resonance.[13]

If we neglect lifetime effects in the phonon dielectric constant, the intensities of the TO phonon Raman lines as a function of hole concentration can be described by

$$L_{\mathrm{TO}} \propto N \int d\vec{q}\, f(\vec{q}) g(\vec{q}) , \tag{12}$$

with $f(\vec{q})g(\vec{q})$ given by Eqs. (5) and (6) or (9) depending on the scattering mechanisms involved. The lines drawn in Fig. 8 were evaluated with Eq. (12), using as a fitting parameter the intensity of the TO-like lines of the sample with 1.6×10^{18} holes cm^{-3}.

In this case of the DP mechanism the hole-concentration dependence of the TO intensities is, according to Eq. (12), approximately proportional to Nq_{TF}^{-1} multiplied by the factors which give the resonant enhancement of the scattering efficiency. The evaluation of Eq. (12) for the IIF mechanism gives a hole-concentration dependence of the TO-like intensities of the type $Nq_{\mathrm{TF}}^{-3} \propto N^{1/2}$.

The calculated intensities account for the different behavior of the DP and IIF mechanisms as well as for the preresonant enhancement with increasing photon energy in the case of the DP mechanism. A good agreement is obtained between the experiment and the calculated intensities for concentrations ranging from 10^8 to 10^9 holes cm^{-3}. Above 10^{19} holes cm^{-3} the calculated intensities are much larger than the experimental ones, a fact which can be attributed to the possible obliteration of the E_1 resonance by the doping.[13,27] The calculated intensities for the case of 1.7×10^{17} holes cm^{-3} are smaller than the measurements due to the presence of some residual scattering, as mentioned before.

CONCLUSIONS

We have presented a detailed study of the coupled LO-phonon—plasmon modes and conclusive evidence of forbidden TO-phonon Raman scattering in heavily doped p-type GaAs. The results of this work together with the investigations reported in Refs. 5—7 show that breakdown of the wave-vector conservation due to scattering by the ionized impurities plays a very important role in the Raman processes in heavily doped semiconductors. A phenomenological model has been proposed to account for the contribution of each wave vector to the total Raman process. The expressions developed to weight these contributions have been used to calculate the hole-concentration dependence of the peak positions, linewidths, and intensities of the measured LO-like and TO-like Raman lines.

ACKNOWLEDGMENTS

The technical assistance of H. Hirt and the help of E. Kisela in sample preparation are gratefully acknowledged.

APPENDIX

The frequency shifts and the broadening of phonons by free carriers can be described as the real and imaginary part of the phonon self-energy, respectively.[24] The frequency shift is given by

$$\hbar\Delta\omega_{\mathrm{TO}} = V^2 P \int \eta(E',q) \times \left[\frac{1}{\hbar\omega_{\mathrm{TO}} - E'} - \frac{1}{\hbar\omega_{\mathrm{TO}} + E'} \right] dE' , \tag{A1}$$

where P stands for the principal part of the integral, $\eta(E',q)$ is the combined density of states for the electronic excitations, and V is the matrix element of the electron-phonon deformation-potential interaction. The linewidth can be decomposed in two contributions:

$$\Gamma = \Gamma_0 + \Delta\Gamma , \tag{A2}$$

with Γ_0 the natural linewidth and $\Delta\Gamma$ the imaginary part of the self-energy which is equal to

$$\hbar\Delta\Gamma = \pi V^2 \eta(\hbar\omega_{\mathrm{TO}},q) . \tag{A3}$$

The matrix element V^2 is given by[24]

$$V^2 = \frac{\hbar d_0^2}{2\rho\omega_{\mathrm{TO}} a_0^2} G(\vec{k},\vec{q}) , \tag{A4}$$

where $\rho = 5.216$ g cm^{-3} is the density of GaAs,

$a_0 = 5.653$ Å the lattice constant, and $d_0 \simeq 48$ eV (Ref. 26) the deformation-potential constant. The factor $G(\vec{k},\vec{q})$ takes into account the fact that the coupling of the valence bands induced by the phonon vibration depends on the relative orientations of the phonon wave vector $\vec{q}$ and that of the electrons $\vec{k}$. Considering only hole excitations within the heavy-hole valence band, a mean value of $\sim\frac{1}{7}$ has been calculated for $G(\vec{k},\vec{q})$ as shown in Ref. 6.

In order to evaluate the shifts and the broadening we have to know the density of states η for the free-particle excitations. For a given wave vector $\vec{q} < 2\vec{q}_F$ the free-particle excitation spectrum extends from 0 to a maximum value given by[22]

$$\Delta E_{\max}(q) = E_F \left[2\frac{q}{q_F} + \frac{q^2}{q_F^2} \right] . \tag{A5}$$

The density of states η for these excitations is proportional to the imaginary part of the Lindhard dielectric function.[22] Its value at the energy E' and for a wave vector $\vec{q}$ depends on the ratios between E' and $E_F \mid 2q/q_F \pm q^2/q_F^2 \mid$. We are interested in the values of η for the wave vector $q_{\max}$ for which $q^2 f(\vec{q}) g(\vec{q})$ has its maximum, with $f(\vec{q})$ and $g(\vec{q})$ given by Eqs. (5) and (6). $q_{\max}$ is tabulated for different hole concentrations in Table III.

In turns out that $\eta(E',q_{\max}) \simeq 0$ for samples with 1.7×10^{17} and 1.6×10^{18} when $E' \simeq \hbar\omega_{\mathrm{TO}}$. Correspondingly, the natural linewidth is measured for these samples. For the samples with 3×10^{18}, 5×10^{18}, and 8×10^{18} holes cm^{-3} the density of states per unit volume at $q_{\max}$ is

$$\eta(E',q_{\max}) = 1.2\times10^3 \frac{q_{\mathrm{TF}}^2}{x} \mid 1-Z^2 \mid \mathrm{cm}^{-3} \times(\text{wave number})^{-1} , \tag{A6}$$

where

$$x = \frac{q_{\max}}{q_F} , \tag{A7}$$

$$Z = \frac{E'}{2E_F x} - \frac{x}{2} . \tag{A8}$$

When the hole concentration exceeds 10^{19} holes cm^{-3} the density of states is given by

$$\eta(E',q_{\max}) = 1.2\times10^3 \frac{q_{\mathrm{TF}}^2}{x} \frac{E'}{E_F} \mathrm{cm}^{-3} \times(\text{wave number})^{-1} . \tag{A9}$$

In Table III the parameters needed to evaluate Eqs. (A6) and (A9) are listed.

[1]For a review, see M. Cardona, in *Proceedings of the 15th International Conference on the Physics of Semiconductors, Kyoto, 1980,* edited by S. Tanaka and Y. Toyozawa [J. Phys. Soc. Jpn. 49, Suppl. A (1980), p. 23].

[2]F. Cerdeira and M. Cardona , Phys. Rev. B 5, 1440 (1972).

[3]F. Cerdeira, T. Fjeldly, and M. Cardona, Phys. Rev. B 8, 4734 (1973).

[4]M. Chandrasekhar, M. Renucci, and M. Cardona, Phys. Rev. B 17, 1623 (1978).

[5]D. Olego, H. Chandrasekhar, and M. Cardona, in *Physics of Semiconductors 1978,* edited by B. L. H. Wilson (Institute of Physics and Physical Society, London, 1979), p. 1313.

[6]D. Olego and M. Cardona, Phys. Rev. B 23, 6592 (1981).

[7]D. Olego, M. Cardona, and U. Rössler, Phys. Rev. B 22, 1905 (1980).

[8]M. V. Klein, in *Light Scattering in Solids,* Topics in Applied Physics, edited by M. Cardona *et al.* (Springer, Berlin, 1975), p. 147.

[9]G. Abstreiter, R. Trommer, M. Cardona, and A. Pinczuk, Solid State Commun. 30, 703 (1979).

[10]W. Cochran, R. Cowley, G. Dolling, and M. Elcombe, Proc. R. Soc. London Ser. A 293, 433 (1966).

[11]A. Pinczuk, G. Abstreiter, R. Trommer, and M. Cardona, Solid State Commun. 30, 429 (1979).

[12]R. Dornhaus, R. Farrow, and R. Chang, Solid State Commun. 35, 123 (1980).

[13]D. Olego and M. Cardona, Solid State Commun. 32, 375 (1979).

[14]W. Richter, in *Solid State Physics,* Vol. 78 of *Springer Tracts in Modern Physics,* edited by G. Höhler (Springer, Berlin, 1976), p. 121.

[15]A. Gogolin and E. Rashba, in *Physics of Semiconductors,* edited by F. G. Fumi (Tipogravia Marves, Rome, 1976), p. 284.

[16]D. Olego and M. Cardona, Phys. Rev. B 22, 886 (1980).

[17]C. Hermann and P. Yu, Phys. Rev. B 21, 3675 (1980).

[18]R. Trommer and M. Cardona, Phys. Rev. B 17, 1865 (1978).

[19]This point of view was not considered in our previous

work about the coupled modes seen in forbidden scattering geometries (Ref. 13). We acknowledge discussion with G. Abstreiter, A. Pinczuk, and W. Richter about this topic.

[20]W. Brinkman and T. Rice, Phys. Rev. B 7, 1508 (1973).

[21]M. Cardona *et al.*, in *Atomic Structure and Properties of Solids,* edited by E. Burstein (Academic, New York, 1972), p. 514.

[22]D. Pines and P. Nozières, *The Theory of Quantum Liquids* (Benjamin, New York, 1966), Vol. 1.

[23]S. Katayama, K. Murase, and H. Kawamura, Phys. Rev. Lett. 33, 1481 (1974).

[24]P. Lawaetz, *The Influence of Holes in the Phonon Spectrum of Semiconductors* (Physics Laboratory III, The Technical University of Denmark, Lyngby, 1978).

[25]L. Pintschovius, J. A. Vergés, and M. Cardona, Proceeding of the International Conference on Phonon Physics, Bloomington, Indiana, 1981 (in press).

[26]M. Grimsditch, D. Olego, and M. Cardona, Phys. Rev. B 20, 1758 (1979).

[27]E. Vigil, J. Rodríguez, and R. Pérez Alvarez, Phys. Status Solidi 90, 409 (1978).